

# A multi-pulse separation reconstruction based on heuristic deconvolution

Georgi Georgiev

Institute for Nuclear Research and Nuclear Energy, Bulgarian Academy of Sciences, BG  
 Physics Faculty, Sofia University “St. Kliment Ohridski”, BG  
 email: georgiev.georgi.st@gmail.com

## Abstract

This study provides a computationally effective heuristic deconvolution algorithm capable to reconstruct piled-up events in loaded scintillator detector systems where fully digitized waveforms are available. A fixed-point iteration algorithm is suggested and used to find properties of the signals which are later used during the signal preprocessing stage. The impulse response function is successfully extracted even from heavily piled-up event waveforms using an iterative approach. A methodology for hit time and amplitude reconstruction is based on a heuristic deconvolution algorithm, which is described in details and some results are presented. The presented algorithms are meant to be general and might be successfully applied to other fields with minor to no modifications.

## I. INTRODUCTION

The present development is inspired by some difficulties in the algorithms for signal reconstruction of the charged particle vetos system of the PADME experiment [1], [2]. The veto system is made of 202 plastic scintillating detectors, read out by silicon photo multipliers (SiPMs) [3]. Tailor made controllers operate the SiPM and pass shaped and amplified signals to CAEN V1742 sampling digitizers, responsible for the data acquisition of the experiment [4].

Event pile up is not rare in the veto system of the PADME experiment which makes the reconstruction a non trivial job. An approach based on the exact impulse response function (IRF) seems inevitable.

Convolution and deconvolution/unfolding algorithms are commonly used in signal processing and for signals from scintillating detectors in particular. These algorithms rather appear in the early stages of the processing as a signal preprocessing or a signal shaping steps [5].

A computationally efficient deconvolution based heuristic algorithm is proposed and studied. The algorithms were initially created with the PADME’s charged particle veto system in mind but they are extendable to other scintillating systems like the small-angle and electromagnetic calorimeters (SAC and ECal) of the PADME experiment [6], [7].

Key preprocessing steps like baseline restoration and spike detection are developed and discussed in the text. The impulse response function is generally not known, but using the suggested robust iterative procedure it can be extracted from the experimental data.

The algorithms are tested with some experimental data from the PADME experiment. Experimental data were also used to obtain the impulse response function of the detectors which is later used to generate synthetic data for the survey of the deconvolution based reconstruction.

## II. SIGNAL PREPROCESSING

The available data from the PADME experiment are sampled at 2.5 GHz with a 12 bits sampling ADC with a dynamic range of 1 V which results to a rescaling divisor 4.096 ADU/mV.

A not fully explained phenomenon leads to a jump in amplitude in the last few samples of the waveforms. In order to eliminate possible complications with the signal reconstruction processing the last 24 samples are substituted with the mean value of the preceding 10 values.

Amplitudes are further calibrated based on the capacitor performances using the algorithm provided in [8].

Additionally spike detection and baseline drift calibration algorithms are applied.

### A. Spike detection

In physics experiments spikes not originating from the studied phenomena are common. These effects for example could be due to a bit flip or a charge leakage caused by ionizing particles interacting with the electronic devices of the data acquisition system. In the experimental data from the PADME experiment single- and double-bin spikes are present.

The following metrics are used to locate single-bin spikes  $M'$  and for double-bin spikes  $M''$ :

$$M'_i = |s_{i+1} - 2s_i + s_{i-1}| - |s_{i+1} - s_{i-1}| \quad (1)$$

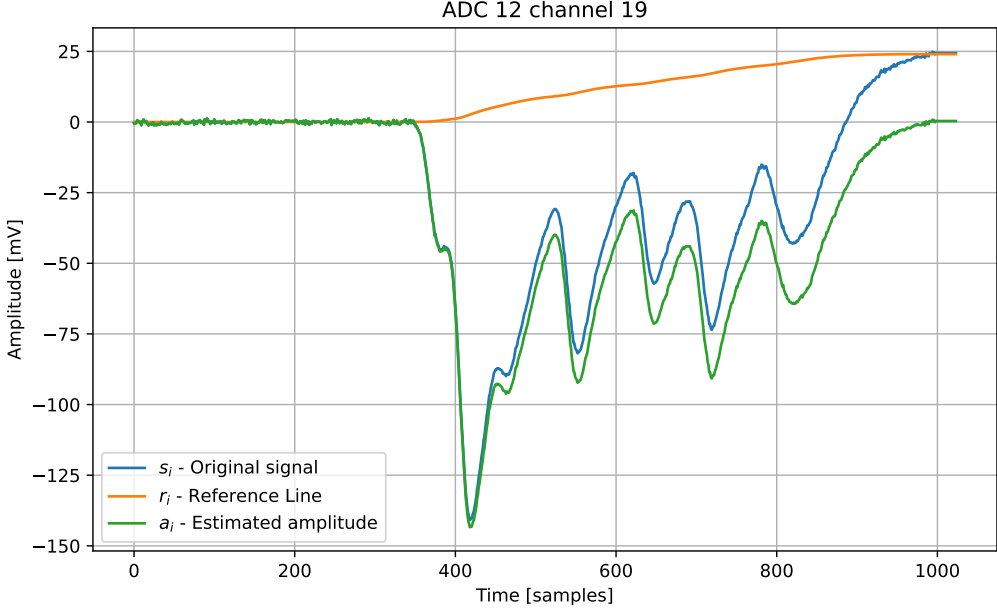


Fig. 1: Illustration of baseline drift calibration.

$$M_i'' = |s_{i+2} - s_{i+1} - s_i + s_{i-1}| - |s_{i+2} - s_{i+1} + s_i - s_{i-1}|, \quad (2)$$

where  $s_i$  is the amplitude of the  $i$ -th sample. The criterion for a spike at  $i$ -th sample is:

$$M_i > 12 \text{ MAD}(M), \quad (3)$$

where  $\text{MAD}(M) = \text{median}_k (|M_k - \text{median}_l(M_l)|)$  is the median absolute deviation of the metric and the threshold 12 is selected experimentally.

These simplistic metrics can fail to determine the exact width of the spike especially if the spikes are located on waveform sections with slopes. The result of the combined  $M'$  and  $M''$  criteria is satisfactory and is used for the purpose of this analysis.

A deconvolution based reconstruction will be relatively insensitive to sporadic spikes as they differ significantly from the impulse response function. On the other hand spikes will be particularly harmful during the process of IRF estimation. For this reason during the IRF estimation events with spikes have been discarded. During the signal reconstruction it is recommended to calculate the corrupted values by linear interpolation of valid neighbouring samples.

### B. Baseline drift

The experimental data show an effect caused by the SiPM controller: waveforms with relatively big number of hits present noticeable drift of the baseline which seems proportional to the cumulative amplitudes (charge) of the waveform. Figure 1 illustrates the baseline drifting effect. This effect is a problem for both IRF estimation and the deconvolution as they assume only sum of offset IRFs and infinite signals so the first and last value should be equal.

The adopted model for the effect is that the change in the reference  $r$  depends on the actual real amplitude  $a$  multiplied with a constant coefficient  $c$ , formally defined using the following difference equation:

$$r_i - r_{i-1} = c \frac{\overbrace{s_i - r_i}^{a_i} + \overbrace{s_{i-1} - r_{i-1}}^{a_{i-1}}}{2} \quad (4)$$

The only known value is  $s$ : the signal measured by the ADC. The constant  $c$  is assumed to be equal for all the channels as the front-end electronics, responsible for this effect, is exactly the same for all veto channels. It is further assumed that:

$$r_0 = s_0 = 0 \quad (5)$$

$$R := r_{1023} = s_{1023} \quad (6)$$

The assumption (5) is valid as the discharge time constant of the front-end electronics is smaller than event time period. The assumption (6) translates to corrected amplitude being zero at the end of the digitization window.  $R$  is used as shorthand for

the last value for the baseline. This assumption, however, is not always satisfied because the relatively long signals from the veto system can go out of the digitization window. The requirement:

$$\min_{i \in [800, 1023]} a_i < -5mV \quad (7)$$

is believed to filter-out all such events.

The constant  $c$  is estimated using the following recurrent algorithm based on fixed-point iteration method. Every new approximation  $c_{new}$ , based on the previous one  $c_{prev}$ , is defined using the relation:

$$c_{new} = \frac{R}{\sum_{i=0}^{1023} s_i - \sum_{i=1}^{1023} \frac{\frac{c_{prev}}{2} s_i + \frac{c_{prev}}{2} s_{i-1} + (1 - \frac{c_{prev}}{2}) r_{i-1}}{1 + \frac{c_{prev}}{2}}} \quad (8)$$

The provided relation tends to overshoot the correct value so the convergence has been accelerated using an exponential moving average:

$$c_{EMA} = \frac{3}{4} c_{new} + \frac{1}{4} c_{prev} \quad (9)$$

Multiple events have been analysed. For each event the constant  $c$  was calculated using the fixed-point iteration. The global value for the constant  $c$  has been found to be:

$$c_{best} = -0.0007134(97).$$

### III. SIGNAL RECONSTRUCTION

The goal is to provide a computationally cheap algorithm that is able to find the timestamps and the amplitudes of hits in the digitized waveforms. Even though Wiener deconvolution with some kind of regularization like the one provided in [9] is possible, it was considered not applicable due to the big amount of data that needs to be processed and the computation cost of the algorithms. An heuristic method for the deconvolution is suggested and tested.

#### A. Impulse response function

The only available information is the digitized waveforms. No theoretical or other a priori estimates are available for the impulse response functions of the detectors or the positions and amplitudes of the hits caused by the interacting charged particles. The impulse response function needs to be extracted from the multiple events with overlapping hits using iterative approach.

1) *Initial guess*: The iterations start from an initial guess defined as:

$$h_0(t) = \text{median} \frac{A_i(t - \arg \min_{\tau} A_i(\tau))}{\min_{\tau} A_i(\tau)}, \quad (10)$$

where  $A_i(t)$  is the  $t$ -th sample of the  $i$ -th signal. This can be visualized as shifting the waveforms so that their absolute minima are located at zero time position then calculate median values for each time position across all waveforms. The motivation is that only the signals from hits with the biggest amplitude will correlate to each other as they are forced to be at same time position. All other signal from hits with smaller amplitudes will appear at random positions. By taking median average an initial approximation for the impulse response function will appear at zero time position and the IRFs caused by other hits will diminish.

2) *Iterations*: Assume

$$s = d * h + \varepsilon, \quad (11)$$

where  $s$  is the digitized waveform,  $d$  is a sparse vector having the hit amplitudes in time,  $*$  denotes convolution,  $h$  is the impulse response function and  $\varepsilon$  is additive noise.

The estimated hits with the current approximation of the impulse response function will be:

$$d_{i,new} = \text{deconvolve}(s_i, h_{prev}), \quad (12)$$

where  $i$  denotes the sequential number of the waveform and *deconvolve* is the heuristic deconvolution method described in section III-B. Then the new approximation for the impulse response function derived from the  $i$  waveforms will be:

$$h_{i,new} = s_i * d_{i,new}^{-1}, \quad (13)$$

where  $d^{-1}$  is the inverse of  $d$  in sense  $d^{-1} = \mathcal{F}^{-1}(1/\mathcal{F}(d))$ .

The differences in hit amplitudes require a maxima based calibration:

$$\bar{h}_{i,t} = \frac{h_{i,t}}{\max_t h_{i,t}} \quad (14)$$

At the end of each iteration an improved version of the impulse response function is calculated as:

$$\hat{h}_{new} = \text{median}(\bar{h}_{i,new}). \quad (15)$$

The robustness of the iterative procedure is demonstrated using only a limited number of piled-up events sample of which is shown on fig. 2a. Even with the absence of a clear picture of the impulse response function within 15 iterations a good estimate was found. The evolution of the IRF estimate is shown on 2b.

### B. Deconvolution

1) *IRF inversion*: The impulse response function  $h$  is a smooth and noiseless function. Taking its inverse  $h^{-1}$  results in huge amplification in the high frequencies. The result is shown on figure 3 with dotted lines. Applying a low-pass filter will remove the high frequency noise at the price of broadening the result of the deconvolution. So instead of sharp lines at the hit position, smooth symmetrical lobes are expected which require further processing. The result with low-pass filter applied  $\tilde{h}^{-1}$  is shown on figure 3 with solid lines.

The spectrum of the estimated impulse response function was studied and it was found that the noise becomes dominant after the 56-th frequency bin.

Low-pass filters based on Blackman-Harris and Hamming windows have been tested with the idea to achieve minimal leakage and narrower main lobe correspondingly. A better result, however, was obtained by applying Hann window corresponding to cut-off frequency 50 MHz at 3 dB illustrated with the dash-dotted line on figure 3. It is handy to store the inverted impulse response function multiplied with the low-pass filter  $\tilde{h}^{-1}$  as it has only 110 non-zero real numbers and can be directly used in the processing of new events by complex multiplication in the frequency domain.

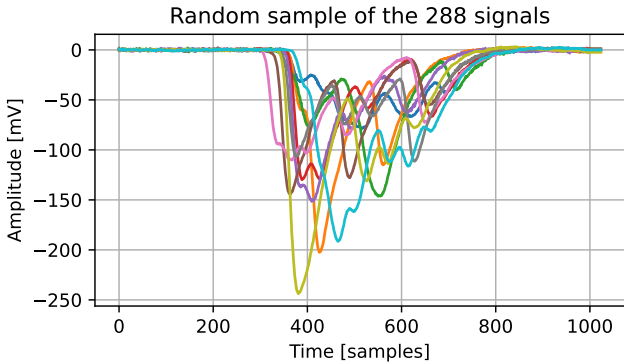
To facilitate the comparison with other algorithms which are using maximal value of the pulse shape as hit amplitude (as opposed to pulse shape integral),  $\tilde{h}^{-1}$  is normalized so that

$$\max_t (h_t * \tilde{h}_t^{-1}) = 1. \quad (16)$$

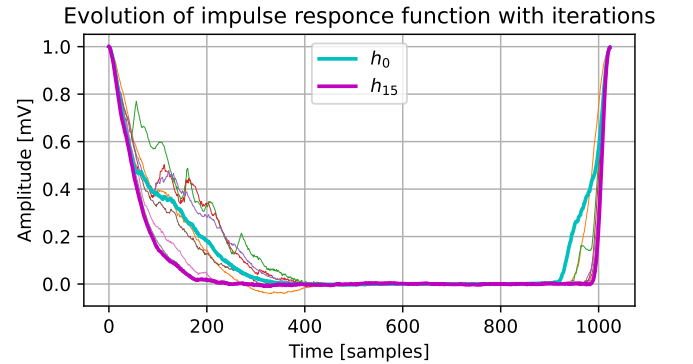
2) *Hit estimate*: The Hann window leakage results in oscillations in the deconvolved signal, which are visible on figure 4. These fluctuations are around the true value—around zero in absence of hits and non-zero in presence of hits. A linear interpolation via the inflection points of the deconvolved signal can be used as a weighting factor: the relative weight of the regions with hits is increased while the oscillations in ranges without hits get suppressed. This heuristic metric is defined as

$$M = q^2 - q \tilde{h}^{-1}, \quad (17)$$

where  $q$  is the linear interpolation between the inflection points of the deconvolved signal  $s * \tilde{h}^{-1}$ . The inflection points are found as the positions of all relative extrema of the successive differences of  $\tilde{h}^{-1}$ .



(a) Waveforms used to test the robustness of the algorithm. The hit signals in all waveforms overlap making it difficult to extract the impulse response function.



(b) The evolution of the estimates for the impulse response function across the iterations is visualized. The initial guess and the final result are shown with thicker lines.

Fig. 2: Illustration of the robustness of the iterative procedure using 288 piled-up events.

The positions of the minima of the resulting metric  $M$  are possible candidates for hit positions. Resulting metric values for all hit candidates are normalized using median absolute deviation. This helps distinguish real hits from the noise. A median value, which is computationally cheaper, can also be used for normalization with similar outcome.

At the moments where the minima of the metric are below the predefined threshold hits is declared. The amplitudes of the hits are the corresponding amplitudes of the deconvolved signal  $h^{-1}$ .

#### IV. PERFORMANCE AND DISCUSSION

In order to better understand the behaviour of the reconstruction algorithm the phase space was sampled using a signal generator. The generated waveforms always have two hits and use the calculated IRF using the iterative algorithm. One is fixed at position 500 and amplitude 550 mV. The position of the other one is varied in the range  $t_{offset} \in [380, 620]$ , which translates to  $\pm 48$  ns time difference with respect to the first hit. The amplitudes of the second hit is varied in the range  $A \in [2, 400]$  mV. Normally distributed Gaussian noise with  $\sigma = 0.55$  mV is added to the signal. The  $\sigma$  value is obtained from experimental data. The synthetic test signal, resembling the experimental waveforms from the PADME veto system, is defined as:

$$s[t] = 550 h[t + 500] + A h[t + t_{offset}] + \mathcal{N}(0, 0.55). \quad (18)$$

The test signals are processed with the presented algorithm to study its performance. Figure 5a shows the number of reconstructed hits. As the test signals have exactly two hits, a single hit corresponds to a false negative, while the three-hit case corresponds to a false positive. An explanation for this behaviour can be found in figure 4 bottom, where the heuristic metric is shown. The peaks of the hits seem to be surrounded by two deep valleys. Thus if a smaller signal occurs within range  $\pm 8$  ns around a bigger hit, it remains undetected. Hits also cannot be detected reliably when their amplitude is smaller than 8 mV. A hit located just next to the valley, tends to be detected as two hits. The algorithm show a dead window which is  $\pm 8$  ns wide. The effect of detecting a single hit as two would not lead to significant problems as they are usually about 1 ns apart.

Figures 5b and 5c show the absolute errors in time of the reconstructed hits for the big hit and for the small hit with varied amplitude respectively. It is visible that the smaller peak causes error in the reconstructed time of the hit with the big amplitude. The deviation of the true value is within  $\pm 1.5$  ns and appears only when a peak with similar amplitude is near by. The reconstructed time for the hit with smaller amplitude shows errors of about few ns when close to a bigger one. This behaviour again is explained with the side lobes that appear in the heuristic metric.

The errors in amplitudes are shown on figures 5d and 5e. Far from other hits the reconstructed amplitudes are within about  $\pm 1\%$  around the true value. When signals are closer than  $\pm 8$  ns the errors in the reconstructed amplitudes become significant. The problems with the reconstructed amplitudes are severe for hits located close to other hits with much bigger amplitudes.

#### V. CONCLUSIONS

The algorithm is computationally cheap, which makes it suitable for processing large amount of events or for online processing. A dead time of  $\pm 8$  ns was observed which is concerning and needs further investigation. The reconstructed amplitudes are correct when hits are not affected by other hits and show significant deviation from the true value when close to other hits.

The algorithms for spike detection and baseline drift correction are important preprocessing steps for the impulse response function estimation, but are, however, independent of the heuristic deconvolution algorithm.

#### ACKNOWLEDGEMENTS

This work is supported by MUCCA, CHIST-ERA-19-XAI-009 / BG-NSF KP-06-D002/4 from 15.12.2020 and funded by The Bulgarian national program “Young scientists and postdocs” RMS 577/17.08.2018 and by Sofia University, Bulgaria.

The PADME collaboration is acknowledged for the ability to test the developed methods on PADME experimental data and for the provision of the physics case which was a main inspiration for this development.

#### REFERENCES

- [1] Raggi M., Kozuharov V., Valente P. The PADME experiment at LNF, *EPJ Web of Conferences* (2015) **96**.
- [2] Raggi M., Kozuharov V. Proposal to Search for a Dark Photon in Positron on Target Collisions at DAΦNE Linac”, *Advances in High Energy Physics*, vol. **2014**, Article ID 959802, 14 pages, 2014.
- [3] F. Ferrarotto et al., Performance of the Prototype of the Charged-Particle Veto System of the PADME Experiment, *IEEE Transactions on Nuclear Science*, vol. 65, no. 8, pp. 2029-2035, Aug. 2018.
- [4] E Leonardi et al. 2017 *J. Phys.: Conf. Ser.* **898** 032024.
- [5] V. Jordanov, Unfolding-synthesis technique for digital pulse processing. Part 1: Unfolding, *NIM-A*, Volume 805, 2016, Pages 63-71
- [6] A. Frankenthal, et al., Characterization and performance of PADME’s Cherenkov-based small-angle calorimeter, *NIM-A*, Volume 919, 2019, Pages 89-97,
- [7] P. Albicocco et al, The International School for Advanced Studies (SISSA), find out more Characterisation and performance of the PADME electromagnetic calorimeter, 2020 *JINST* 15 T10003
- [8] Georgi Georgiev for the PADME collaboration 2022 *J. Phys.: Conf. Ser.* 2255 012008, doi: 10.1088/1742-6596/2255/1/012008
- [9] Selesnick I., Sparce deconvolution (an MM algorithm), Polytechnic Institute of New York University, (2014)

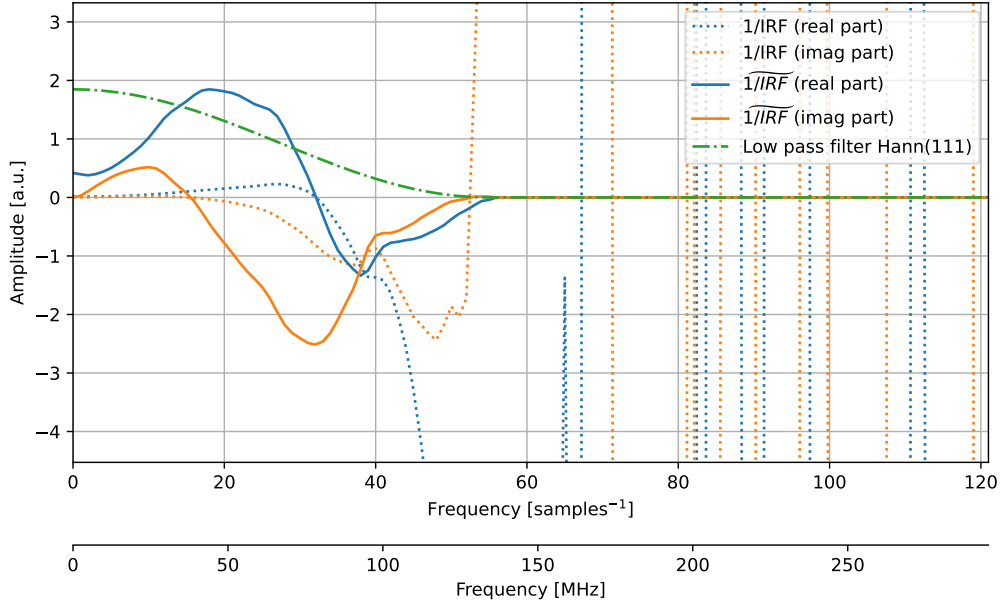


Fig. 3: The real and imaginary part of the inverse of the impulse response function  $h^{-1}$  are shown with dotted line. The dash-dotted line shows the spectrum of the low-pass filter. The solid lines represent the inverse of the impulse response function with the low-pass filter applied  $\widetilde{h^{-1}}$ .

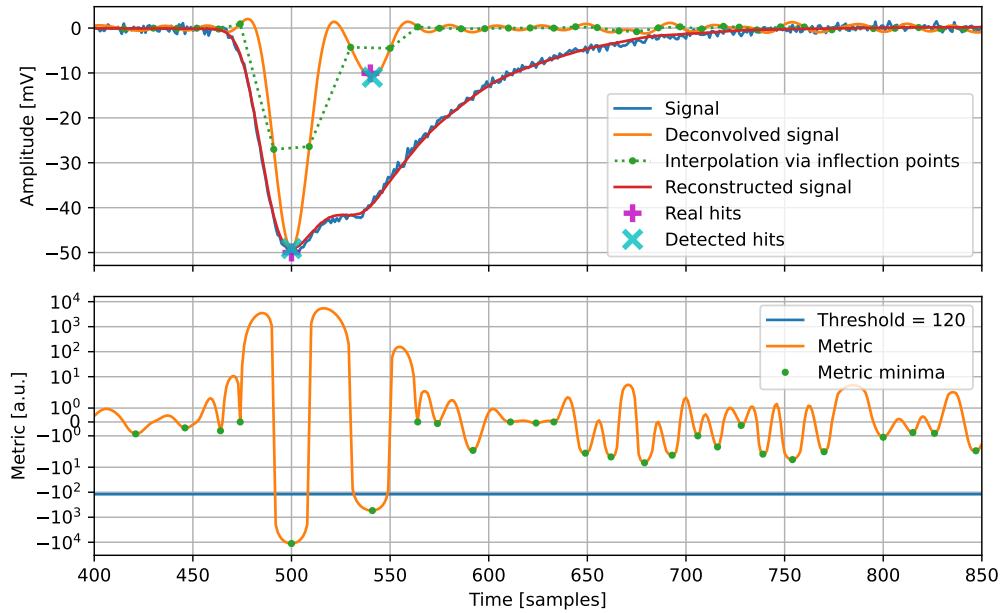
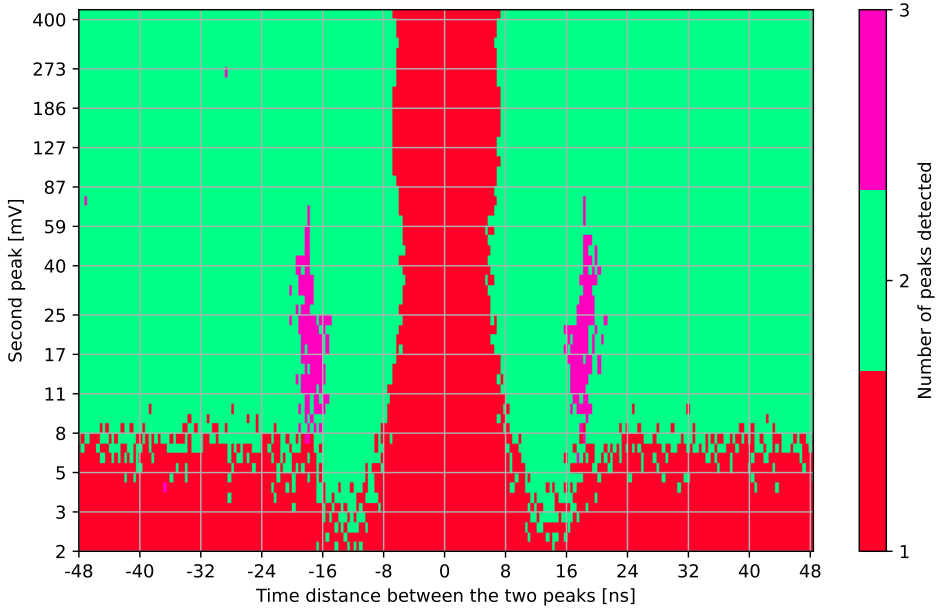
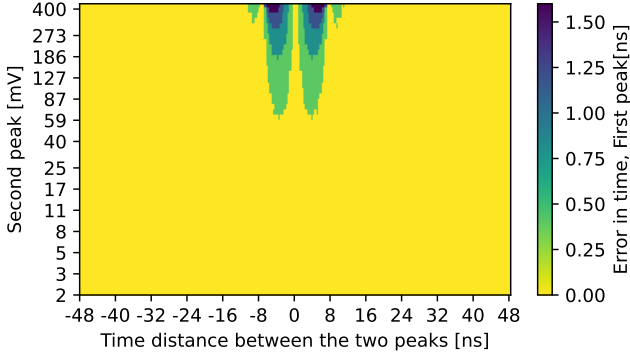


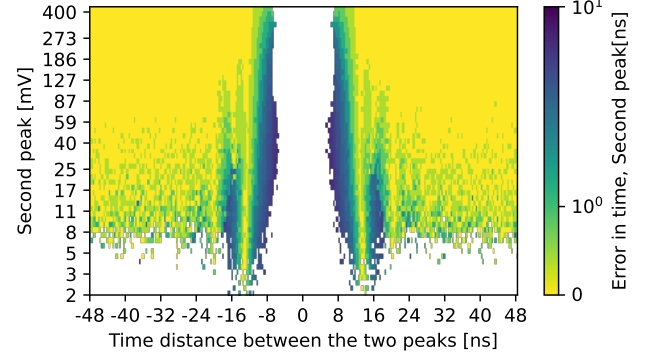
Fig. 4: Deconvolution example using artificially generated signal. True and reconstructed signals are plotted together with other functions involved in the deconvolution process.



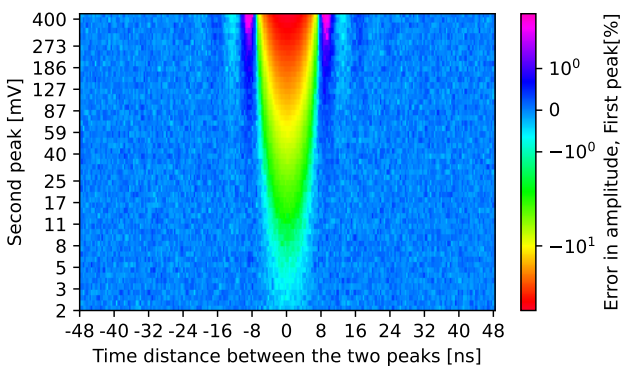
(a) The map shows the detected number of hits for each pair amplitude / time offset.



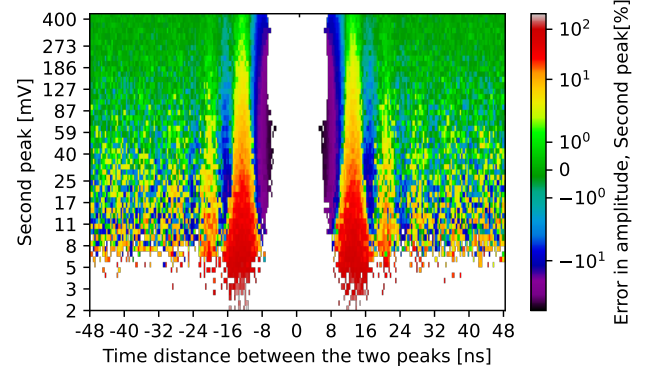
(b) Errors in the reconstructed time of the hit with bigger amplitude.



(c) Errors in the reconstructed time of the hit with varied amplitude.



(d) Errors in the reconstructed amplitude of the hit with bigger amplitude.



(e) Errors in the reconstructed amplitude of the hit with varied amplitude.

Fig. 5: Performance of the proposed reconstruction algorithm using artificially generated events. The generated waveforms have exactly two signals: one fixed at position and amplitude and a second with variable position and amplitude